Journal of Molecular Spectroscopy **205,** 185–196 (2001)
doi:10.1006/jmsp.2000.8263, available online at http://www.idealibrary.com on IDEAL®

The Rotational–Torsional Spectrum of the *g′Gg* Conformer of Ethylene Glycol: Elucidation of an Unusual Tunneling Path

D. Christen,* L. H. Coudert,† J. A. Larsson,‡ and D. Cremer‡

**Institut für Physikalische und Theoretische Chemie, Universität Tübingen, Auf der Morgenstelle 8, D-72076 Tübingen, Germany; †Laboratoire de Photophysique Moléculaire, CNRS, Bâtiment 210, Université de Paris-Sud, 91405 Orsay Cedex, France; and ‡Department of Theoretical Chemistry, Göteborg University, Reutersgatan 2, SE-41320 Göteborg, Sweden*

Received May 8, 2000; in revised form October 17, 2000

The microwave spectrum of the energetically unfavored *g′Gg* conformer of ethylene glycol (CH_2OH—CH_2OH) is reported. This spectrum is dominated by an interconversion geared-type large-amplitude motion during which each OH group in turn forms the intramolecular hydrogen bond. The microwave spectrum has been analyzed with the help of a Watson-type Hamiltonian plus a 1.4-GHz tunneling splitting. The rotational dependence of this tunneling splitting has been examined using an IAM approach and this yielded qualitative information on the tunneling path the molecule uses to interconvert between its two most stable conformers. Unexpectedly, but in agreement with *ab initio* calculations, when tunneling occurs between the energetically equivalent *g′Gg* and *gGg′* conformers, the OH groups are rotated stepwise through 240° in the sense of a flip-flop rather than a concerted rotation and the molecule goes through the more stable *g′Ga* and *aGg′* forms. The electronic reasons for preferring a long rather than a short rotational path via a *gGg* form are discussed using calculated adiabatic vibrational modes.

Key Words: ethylene glycol; microwave; spectrum; conformer; large-amplitude motion; tunneling path; *ab initio* calculation.

1. INTRODUCTION

Ethylene glycol is a member of an interesting class of triple rotor molecules principally capable of establishing different conformers and of performing large-amplitude motions. The coupled rotation around the CC bond and the two CO bonds can lead to a complex conformational behavior which was partly elucidated by experimental as well as theoretical means including microwave spectroscopy (*1–5*), electron diffraction (*6*), vibrational spectroscopy (*7*), and quantum chemical calculations (*6, 8–22*). For a threefold rotational potential and three rotor groups, $3^3 = 27$, distinct conformations can be differentiated, which because of symmetry reduce to 10 (see Fig. 1), namely, six forms with an *anti* (*A*) arrangement of the OH groups and four with a *gauche* (*G*) arrangement. It is well-known that in 1,2-disubstituted ethanes the *G* forms are mostly more stable than the *A* forms[1] because the *gauche* effect (*23*) is of importance for a molecule with electronegative substituents. In the case of ethylene glycol, there is in addition the possibility of intramolecular H bonding, which may add to the stability of a *G* conformer. Of the 10 forms shown in Fig. 1, only the *g′Ga* and the *g′Gg* forms can establish intramolecular hydrogen bonds, and in the gas phase these two conformers are expected to be energetically favored.

[1] We denote rotomers by capital letters *A* or *G* with regard to rotation at the CC bond and by lowercase letters *a* or *g* with regard to rotation at the CO bonds where clockwise/counterclockwise rotation is indicated by a positive/negative dihedral angle and the symbols *g*/*g′*. The rotational directions are determined by looking along the CC and the CO axes from the first to the second atom.

Indeed, the microwave spectra of only two conformers have been identified so far (*1–5*). In Ref. (*1*), the microwave spectrum of the *g′Ga* conformer of the bideuterated $DOCH_2CH_2OD$ isotopomer could be assigned and analyzed, while in Ref. (*2*), for the same conformer, the microwave spectrum of the asymmetrically substituted monodeuterated isotopomer $DOCH_2CH_2OH$ was observed. The first spectrum of the *g′Gg* conformer was recorded later (*3*) for the asymmetrically substituted bideuterated isotopomer $HOCH_2CD_2OH$. However, the microwave spectrum of the normal species (*4*) remained unassigned for a long time. It was only in 1995 (*5*) that the first transitions of the *g′Ga* conformer were identified. In this species a large-amplitude coupled rotation of the two hydroxyl groups heavily perturbs the spectrum and leads to a 7-GHz tunneling splitting. The energy-level pattern is significantly altered from that of a rigid rotor and the assignment would not have been possible without two very selective and powerful techniques: molecular bean Fourier transform microwave spectroscopy (MBFTMW) and microwave–microwave double-resonance spectroscopy (MWMWDR). The former technique allows for the identification of transitions with low *J* values (due to rotational temperatures in the range of a few kelvins) and the latter only records a signal in the case that two frequencies simultaneously fit into a three-level system (two transitions share a common level). In order to account for the perturbations due to the tunneling process, a theoretical model was formulated, based on the internal axis method (IAM) developed for multidimensional tunneling (*24, 25*). This method allowed for a satisfactory reproduction of the observed frequencies of both the normal and bideuterated *O–d*$_2$ species of the *g′Ga* conformer (*5*).

0022-2852/01 $35.00

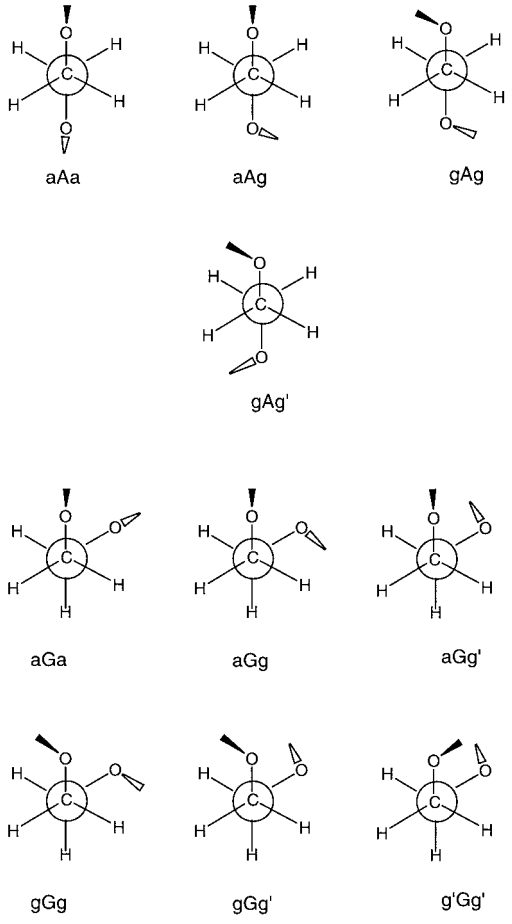

FIG. 1. The 10 possible *A* and *G* conformations of ethylene glycol shown in form of Newman projections. The main differences between these conformers lay in their HOCO and OCCO dihedral angles.

Thus the analytical model was available to start the search for the energetically less favorable (*3*) hydrogen-bonded conformer $g'Gg$ and to describe its rotational behavior. For this purpose, a two-pronged strategy was followed by combining MW measurements with quantum chemical calculations. On the basis of these investigations, we are able to present the microwave spectrum of the normal species of the $g'Gg$ conformer, to discuss its relative stability, and to predict its most likely conversion modes on the conformational energy surface (CES). Last, we will show that results of the analysis of the microwave spectrum and of the *ab initio* calculations lead to the same description of the conformational behavior of ethylene glycol.

2. COMPUTATIONAL DETAILS

Both density functional theory (DFT) (*26, 27*) and second-order Møller–Plesset (MP2) theory (*28*) were used to describe the rotational behavior of *G*-ethylene glycol. Preliminary geometry optimizations and vibrational frequency calculations were performed with the B3LYP exchange-correlation hybrid functional (*29*) employing Poples 6-31G(d, p) basis set (*30*). However, DFT is known to describe H bonding in a satisfactory way provided the basis set has at least TZP quality (*31*). Also, in recent work (*32*) it was found that even B3LYP/6-311+G(d, p) may lead to an unreasonable description of H bonding, which was confirmed in the present work. Therefore, B3LYP geometries were used as starting geometries for the more reliable MP2/6-311G(d, p) geometry optimizations and vibrational frequency calculations.

The convergence criteria of the geometry optimization were set to 10^{-5} atomic units for the rms error of the calculated atom displacements and the rms error of the calculated forces exerted on the atoms. In this way, calculated distances and angles can be expected to be numerically accurate to 10^{-4} Å and 0.01 degree.

Calculated vibrational modes were investigated using the adiabatic internal mode (AIM) analysis of Refs. (*33, 34*). This approach is based on a decomposition of normal modes in terms of adiabatically relaxed internal parameter modes that are not contaminated by any other mode of the molecule. As has been shown previously (*35*), the adiabatic mode analysis is superior to the potential energy distribution (PED) analysis and provides reliable internal frequencies and internal force constants that can directly be assigned to the internal parameters of a molecule (*36*). In this work, the adiabatic modes will be used to describe H bonding and to rationalize the preferred rotational mode of *G*-ethylene glycol.

For all molecules considered, zero point energy (ZPE), thermal corrections, and entropies S were determined to evaluate relative enthalpies $\Delta H(298)$ and relative free enthalpies (Gibbs energies) $\Delta G(298)$ at 298 K. Calculations were carried out with the *ab initio* packages COLOGNE99 (*37*) and GAUSSIAN98 (*38*).

3. ASSIGNMENT OF THE SPECTRUM

As the experimental setup for the MWMWDR experiment and for the MBFTMW pulsed spectrometer used for the present measurements are the same as those used in our previous paper (*5*), the reader is referred to that paper for a detailed description of these spectrometers.

The $g'Gg$ conformer was already identified in two asymmetrically substituted ethylene glycol isotopomers (*3*), thus the question for the normal species was not whether, but how, to find this conformer.

The first step in the search for this second conformer was a least-squares refinement of the structure based on *ab initio* calculations. Starting from the *ab initio* model, seven parameters were fitted to rotational constants of the $g'Ga$ conformer from the normal to the bideuterated species (*1–3*), the molecules being $HOCH_2CH_2OH$, $DOCH_2CH_2$**OH**, $HOCH_2CH_2$**OD**, $HOCH_2$-CD_2**OH**, **HO**CH_2CD_2OH, and $DOCH_2CH_2OD$, where for non-

TABLE 1
Structural Parameters for the $g'Ga$ and $g'Gg$ Conformers of Ethylene Glycol

	$g'Ga$		$g'Gg$			$g'Ga$		$g'Gg$	
Parameter[a]	*ab initio*[b]	Fit[c]	*ab initio*[b]	Model[d]	Parameter[a]	*ab initio*[b]	Fit[c]	*ab initio*[b]	Model[d]
C_0–C_1	1.5124		1.5159		$\angle H_2C_0C_1$	108.75		109.08	
C_1–O_7	1.4259	1.4385	1.4262	1.4388	$\angle H_5C_1C_0$	110.57		111.09	
C_0–O_6	1.4135	1.4138	1.4123	1.4126	$\angle H_3C_1C_9$	108.68		109.39	
C_0–H_4	1.0923		1.0930		$\angle H_9O_7C_1$	107.38	106.40	106.39	105.41
C_0–H_2	1.0987		1.1021		$\angle H_8O_6C_0$	103.98		104.29	
C_1–H_5	1.0977		1.0975						
C_1–H_3	1.0964		1.0911		$\angle O_6C_0C_1O_7$	60.96	60.80	57.04	56.88
O_7–H_9	0.9579		0.9604		$\angle H_4C_0C_1O_7$	179.47		175.99	
O_6–H_8	0.9617		0.9622		$\angle H_5C_1C_0O_6$	181.76		181.25	
					$\angle H_2C_0C_1O_7$	−61.76		−65.50	
$\angle O_7C_1C_0$	105.88	108.08	110.01	112.21	$\angle H_3C_1C_0O_6$	−58.21		−58.45	
$\angle O_6C_0C_1$	110.64		110.47		$\angle H_9O_7C_1C_0$	197.35	196.57	69.12	67.97
$\angle H_4C_0C_1$	110.10		110.59		$\angle H_8O_6C_0C_1$	310.17	295.57	316.99	302.39

[a] In this column the structural parameters are given. Bond distances and bond angles are respectively given in Å and degree units. The atom numbering is defined in Fig. 2.

[b] Values obtained for the structural parameters through the *ab initio* calculations are reported in this column.

[c] In this column, values obtained for some of the structural parameters of the $g'Ga$ conformer by fitting the rotational constants are given. A blank entry means that the corresponding parameter was not varied.

[d] The values for the structural parameters of the $g'Gg$ conformer listed in this column were obtained maintaining their difference with the calculated (*ab initio*) values equal to those for the $g'Ga$ conformer.

equivalent hydroxyl groups the one in bold script partakes in the hydrogen bond.

The following parameters were allowed to vary: two CO bond lengths, one CCO bond angle, the OCCO dihedral angle, and two CCOH dihedral angles, as well as one COH bond angle. The mean deviation of the rotational constants for this model of the $g'Ga$ conformer was less than 6 MHz.

These refined values of the structural parameters were exported to the $g'Gg$ conformer maintaining the calculated (*ab initio*) differences between the two conformers. The resulting model was tested by comparison of the predicted rotational constants with those of the two asymmetrically substituted isotopomers that had already been identified (*3*). Based on these deviations, a set of rotational constants were finally predicted for the normal species of the $g'Gg$ conformer. The structural parameters for the two conformers are shown in Table 1 and the predicted rotational constants for the $g'Gg$ conformer are shown in Table 2. The atom numbering used to identify the structural parameters in Table 1 is defined in Fig. 2 for both the $g'Ga$ and the $g'Gg$ conformers.

However, even with a presumably good model, the experimental part of this investigation still posed problems. The spectrum is very crowded in all regions and since even the search for characteristic transitions of the energetically favored conformer ($g'Ga$) failed to yield an assignment, albeit under different circumstances and with a weaker model, an analysis of the stark spectrum in order to identify transitions belonging to the $g'Gg$ conformer did not seem very promising.

Use of the double-resonance technique had proven itself invaluable by the search for and assignment of transitions

TABLE 2
Rotational Constants for the $g'Ga$ and $g'Gg$ Conformers of Ethylene Glycol

Rotational Constants[a]	Analysis[b]	Fit[c]	Model[d]	Corr. Model[e]
A	15 363.28	15 354.38	15 173.30	15 193
B	5 587.10	5 593.59	5 556.24	5 538
C	4 613.54	4 616.01	4 604.71	4 595

[a] All rotational constants are given in MHz.

[b] For the $g'Ga$ form, from the analysis reported in Ref. (*5*).

[c] Calculated for the $g'Ga$ form from the structural parameters reported in Table 1 in the columns headed 'Fit.'

[d] Calculated for the $g'Gg$ form from the structural parameters reported in Table 1 in the columns headed 'Model.'

[e] Calculated for the $g'Gg$ form from the structural parameters reported in Table 1 in the columns headed 'Model' and corrected after comparison with $HOCH_2CD_2\mathbf{OH}$ and $\mathbf{HO}CH_2CD_2OH$ (see text).

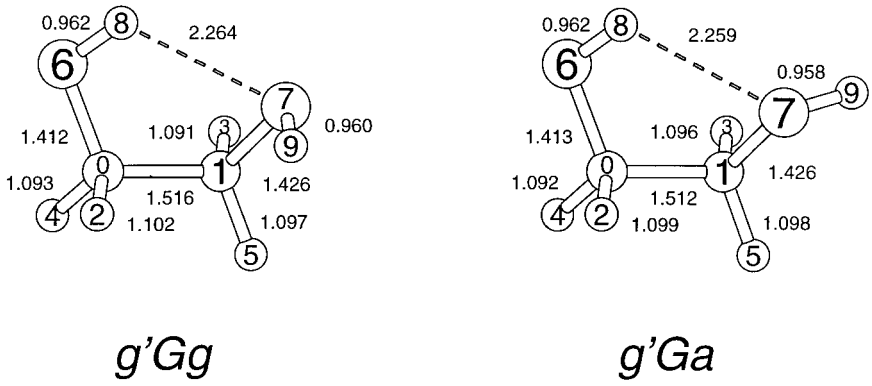

FIG. 2. The two conformers $g'Gg$ and $g'Ga$ of ethylene glycol which are connected by the large-amplitude coupled torsion of the OH groups are shown. In addition to the atom numbering, some of the bond distances obtained by *ab initio* calculations are also given. The complete set of internal coordinates calculated at the MP2/6-311G(*d*, *p*) level of theory is given in Table 1.

belonging to the $g'Ga$ conformer, but the trouble with the present DR setup is the very low radiation density and, as a result of this, a double-resonance cross-sectional depth of only a few megahertz at the absolute powers applied for the pumping radiation (~1 W). Thus DR is of great benefit with likely candidates for a DR search but extremely time consuming (at this cross-sectional depth) without such candidates, which left MBFTMW as the last one out.

It would not be practical to suggest the use of a supersonic molecular beam technique for the search for an energetically *unfavored* conformer (*3*), except that this matter really depends on the shape of the potential hypersurface (*39*). If the molecules in the molecular beam are basically adiabatically cooled to rotational temperatures of a few kelvins, some molecules will end up in the ground state of the energetically unfavored conformer and will then be available for the FTMW experiment. If the cooling is basically diabatic, however, or the barrier between the two conformers rather low, all molecules will probably end up in the ground state of the energetically favored conformer.

We decided to take the chance using MBFTMW spectroscopy and asked A. Hight Walker and R. D. Suenram, Molecular Physics Division, NIST, who had taken part in the investigation of the $g'Ga$ conformer of ethylene glycol (*5*), to help out. In Ref. (*4*) it was explained for the $g'Ga$ conformer that an interchange of the two hydroxyl groups conserves the sign of the *b* component of the dipole moment, whereas it changes the sign of its *a* and *c* components. This is also true for the $g'Gg$ conformer. If we assign the quantum number $v = 0$ or $v = 1$, respectively, to the lower and upper sublevels arising from the tunneling through the concerted torsion barrier, the most easily recognizable part of the spectrum will be the (perhaps slightly distorted) $\Delta v = 0$ rigid-rotor *b*-type spectrum, probably consisting of narrow doublets ($v = 0$ or $v = 1$ sublevels), whereas the $\Delta v = 1$ *a*- and *c*-type transitions will be split by an at first unknown amount, depending on the shape of the barrier. The MBFTMW search was therefore initiated in order to identify low *J* *b*-type transitions in the 10–20 GHz region, guided by model calculations with the predicted rotational constants.

A first look at the MBFTMW spectrum in the 10.4–12.0 GHz region did not seem to provide much ground for optimism. The spectrum shows three doublets that all belong to the $g'Ga$ conformer: $2_{02} \leftarrow 1_{11}$ ($v = 1$ at 10 534.513, $v = 0$ at 10 551.877 MHz), $1_{10} \leftarrow 1_{01}$ ($v = 0$ at 10 747.533, $v = 1$ at 10 754.257 MHz), and $2_{11} \leftarrow 2_{02}$ ($v = 0$ at 11 785.804, $v = 1$ at 11 810.300 MHz). Digital erasure of the strongest lines and subsequent amplification of the rest spectrum did, however, reveal the presence of weak lines that definitely did not belong to the $g'Ga$ spectrum. One should be aware, of course, that the sensitivity of the method at this scale of amplification allows for the detection of lines belonging to the ^{13}C isotopomers of the $g'Ga$ conformer, but a couple of weak transitions seemed to correspond very well with the predicted *b*-type spectrum of the $g'Gg$ conformer: the $1_{10} \leftarrow 1_{01}$ transition, predicted at 10 598 MHz and observed at 10 618.526 and 10 619.115 MHz; the $2_{11} \leftarrow 2_{02}$ transition, predicted at 11 608 MHz and observed at 11 628.931 and 11 629.509 MHz; and the $1_{11} \leftarrow 0_{00}$ transition, predicted at 19 788 MHz and observed at 19 809.432 and 19 811.497 MHz. Using these three transitions in a rigid-rotor fit refined the rotational constants of the model and allowed for a more precise prediction of the $3_{12} \leftarrow 3_{03}$ transition. It was predicted at 13 260.0 MHz and observed at 13 261.040 and 13 263.449 MHz. With these four sets of lines, a sound basis for a double-resonance search had been established. As by the analysis of the $g'Ga$ spectrum, the search for DR signals at first concentrated on *b*-type transitions, pumping the already identified (MBFTMW) transitions. Table 3 gives the pump and probe transitions of the initial DR search.

Eventually the search was extended to cover *a*- and *c*-type transitions, at first pumping already identified *b*-type transitions. So far 180 transitions with a maximum *J* of 7 have been assigned. The frequencies are listed in Table 4 and the resulting spectroscopic parameters are listed in Table 5. The energy level diagram for $0 \leq J \leq 3$ with measured pump and signal

TABLE 3
Results of the Microwave–Microwave Double Resonance Experiment

Pump Transition[a]	Pump Frequency[b]	Signal Transition[a]	Signal Frequency[b]
$v=0, 1_{10} \leftarrow 1_{01}$	10618.53	$v=0, 2_{12} \leftarrow 1_{01}$	29003.38
"	"	$v=0, 2_{21} \leftarrow 1_{10}$	50242.96
$v=1, 1_{10} \leftarrow 1_{01}$	10619.11	$v=1, 2_{12} \leftarrow 1_{01}$	28995.98
"	"	$v=1, 2_{21} \leftarrow 1_{10}$	50235.09
$v=0, 2_{02} \leftarrow 1_{11}$	10524.45	$v=0, 2_{20} \leftarrow 1_{11}$	51249.28
"	"	$v=0, 3_{13} \leftarrow 2_{02}$	37749.87
$v=1, 2_{02} \leftarrow 1_{11}$	10522.13	$v=1, 2_{20} \leftarrow 1_{11}$	51242.79
"	"	$v=1, 3_{13} \leftarrow 2_{02}$	37739.60
$v=0, 2_{11} \leftarrow 2_{02}$	11629.51	$v=0, 2_{20} \leftarrow 2_{11}$	29095.33
$v=1, 2_{11} \leftarrow 2_{02}$	11628.93	$v=1, 2_{20} \leftarrow 2_{11}$	29091.69
$v=0, 3_{12} \leftarrow 3_{03}$	13261.04	$v=0, 4_{14} \leftarrow 3_{03}$	46137.09
"	"	$v=0, 3_{21} \leftarrow 3_{12}$	27984.52
$v=1, 3_{12} \leftarrow 3_{03}$	13263.45	$v=1, 4_{14} \leftarrow 3_{03}$	46123.06
"	"	$v=1, 3_{21} \leftarrow 3_{12}$	27979.77

[a] The assignment of the transition is given in this column in terms of a vibrational quantum number, identical for the upper and lower levels, and in terms of rotational quantum numbers.
[b] Frequencies are given in MHz.

lines are drawn in Fig. 3. The rotational constants (including centrifugal distortion) do not deviate markedly from those of the $g'Ga$ conformer, but the tunneling splitting is only 1.4 GHz compared to 7 GHz in the $g'Ga$ conformer. Thus either the barrier height in the $g'Gg$ conformer may be considerably higher than the one in the $g'Ga$ conformer or the tunneling path may be "longer," i.e., the barrier is wider. The results of Section 6 seem to confirm this latter hypothesis.

4. THE CONFORMATIONAL ENERGY SURFACE

In the present investigation, the torsional angles $\xi_1 = \angle H_8O_6C_0C_1$ and $\xi_2 = \angle H_9O_7C_1C_0$ will be used to characterize the different conformations of ethylene glycol. They differ from those used in the previous paper (*5*) by a 180° additive factor. Figures 4 and 5 give a schematic representation of a part of the periodic conformational energy surface (CES) spanned by the angles ξ_1 and ξ_2. The $g'Gg$ conformer which will be labeled **1** is close to the point $(\xi_1, \xi_2) = (-60, 60)$ and can rotate into the gGg' conformer, labeled **2**, by a concerted disrotatory motion of the two OH groups as indicated by the dashed line in Fig. 4. However, this would imply a high-energy process since the aGa form has to be passed, which because of lone pair–lone pair repulsion possesses a relatively high energy. For the same reason, the concerted conrotatory interconversion between gGg and $g'Gg'$ forms (see Fig. 4) is also unlikely. *G*-ethylene glycol can avoid the concerted paths by a nonconcerted flip-flop rotation, in which first one of the OH groups rotates from a g to a g' position and, then, the other OH group follows by a rotation from the g' to the g conformation. By the sequence of OH rotations, two paths are defined on the CES: Path *A* corresponding to a (0, 240)–(240, 0) flip-flop process from conformation **1** to conformation **2** in which the second OH group, the position of which is characterized by ξ_2, rotates first. Path *B* represents a shorter (120, 0)–(0, 120) flop-flip rotation from **1** to **2** (lower left corner of Fig. 4), in which the sequence of OH rotations is changed.

Both paths lead to transient forms. Path *A* goes through the $g'Gg'$ form; path *B* through the gGg (see Figs. 4 and 5, in which intramolecular H bonding is no longer possible and which therefore should be higher in energy than any of the H-bonded conformations). *A priori*, it is difficult to see whether H,H repulsion as in the $g'Gg'$ form or lone pair–lone pair repulsion as in the gGg form are more destabilizing. A prediction based on the least-motion principle would suggest path *B* to be more likely, in particular since the effective barrier for H tunneling should be smaller for this path. Hence, it is another goal of this work to clarify whether path *A* or path *B* is preferred for the interconversion between $g'Gg$ conformers.

5. ANALYSIS OF THE SPECTRUM AND TUNNELING PATHS

As pointed out in the introduction, the $g'Ga$ and $g'Gg$ conformers of glycol both display a large-amplitude motion which significantly alters their rotational energy levels and prevents the use of a Watson-type Hamiltonian to calculate their spectra. For this reason a theoretical model was developed in the previous investigation (*5*). In the present investigation there is no need to reformulate a theoretical model because the $g'Gg$ and $g'Ga$ conformers display the same kind of large-amplitude motion which, as described in the previous sections, corresponds to rotations of the two hydroxyl groups with respect to the CO bonds. More precisely, from the point of view of symmetry, both conformers are equivalent. When the $g'Gg$ conformer tunnels along one of the tunneling paths described previously, the symmetry relations obeyed by the reference position of the atoms are the same as in the case of the $g'Ga$ conformer and this means that Eq. [2] of Ref. (*5*) is also valid in the present case. For that reason, the results given in Section 4.C of Ref. (*5*) can be readily used in this investigation and the reader is referred to that paper for further information.

The assigned transitions of the $g'Gg$ conformer were included in a least-squares fit procedure where transitions were given a weight equal to the square of the inverse of their experimental uncertainty. The parameters of Eqs. [8]–[10] and [14] of Ref. (*5*) were fitted to the experimental frequencies. Table 4 lists the assignment, the observed frequency, and the observed minus calculated difference for each transition.

Table 5 gives the values of the spectroscopic parameters

TABLE 4

Assignments, Frequencies, and Observed Minus Calculated Differences in the Microwave Spectrum of the *g′Gg* Conformer of Glycol

J'	K_a'	K_c'	v'	J''	K_a''	K_c''	v''	Obs[a]	Diff[b]	J'	K_a'	K_c'	v'	J''	K_a''	K_c''	v''	Obs[a]	Diff[b]
3	1	2	1	3	1	3	0	7012.500(500)	−7	5	1	5	0	4	2	2	0	11830.900(500)	−48
2	1	2	0	2	0	2	1	7438.200(500)	34	5	1	4	0	5	1	5	1	12720.000(500)	235
4	1	4	1	4	0	4	0	7584.600(500)	−163	4	1	3	0	3	2	1	1	12938.800(500)	102
6	2	5	0	5	3	3	1	7871.700(500)	10	3	1	2	0	3	0	3	0	13261.040(10)	−3
4	1	3	0	4	1	4	1	8059.400(500)	477	3	1	2	1	3	0	3	1	13263.449(10)	−24
2	0	2	0	1	1	0	1	8216.900(500)	3	6	2	4	0	5	3	3	0	13402.100(500)	403
5	4	1	0	6	3	3	1	8217.700(500)	−417	6	2	4	1	5	3	3	1	13403.700(500)	680
1	1	1	0	1	0	1	1	8311.740(500)	180	5	1	5	1	4	2	3	0	14118.900(500)	−100
5	4	2	0	6	3	4	1	8451.700(500)	−107	4	1	3	0	3	2	2	0	14619.100(500)	123
1	0	1	0	0	0	0	1	8766.080(500)	−440	4	1	3	1	3	2	2	1	14621.700(500)	326
3	1	3	1	3	0	3	0	8961.700(500)	−174	6	2	4	1	5	3	2	0	14662.600(500)	257
6	2	5	0	5	3	2	0	9131.300(500)	287	5	1	4	1	5	1	5	0	15404.900(500)	−170
5	4	2	0	6	3	3	0	9548.700(500)	−530	4	1	3	0	4	0	4	0	15644.000(500)	315
5	4	1	1	6	3	4	1	9781.800(500)	−355	4	1	3	1	4	0	4	1	15650.500(500)	−11
5	4	1	0	6	3	4	0	9783.500(500)	−205	4	1	3	1	3	2	1	0	15652.200(500)	200
2	1	2	1	2	0	2	0	10159.880(500)	−36	3	0	3	0	2	1	1	1	17148.900(500)	124
2	0	2	1	1	1	1	1	10522.130(500)	−104	6	1	6	1	5	2	3	1	17577.300(500)	−89
2	0	2	0	1	1	1	0	10524.450(10)	−35	6	1	6	0	5	2	3	0	17602.200(500)	−196
6	2	5	1	5	3	3	0	10538.000(500)	208	2	1	2	0	1	1	1	1	17960.400(500)	0
1	1	0	0	1	0	1	0	10618.526(10)	−26	1	1	0	0	0	0	0	1	19385.034(10)	−38
1	1	0	1	1	0	1	1	10619.115(10)	−33	1	1	1	1	0	0	0	1	19809.432(10)	−23
4	1	3	1	4	1	4	0	10760.900(500)	444	1	1	1	0	0	0	0	0	19811.497(10)	−16
5	4	1	1	6	3	3	0	10878.900(500)	−677	2	1	1	0	1	1	0	1	19846.423(10)	15
2	0	2	1	1	1	0	0	10946.700(500)	83	2	1	2	1	1	1	1	0	20684.382(10)	−19
1	1	1	1	1	0	1	0	11042.922(10)	−13	2	0	2	1	1	0	1	0	21565.280(50)	111
5	4	2	1	6	3	4	0	11111.700(500)	−522	2	1	1	1	1	1	0	0	22575.610(50)	33
5	1	5	0	4	2	3	1	11432.500(500)	−181	5	2	4	1	5	1	4	0	25018.820(50)	−49
1	0	1	1	0	0	0	0	11499.966(10)	13	4	0	4	0	3	1	2	1	25274.790(50)	−83
2	1	1	1	2	0	2	1	11628.931(10)	−28	5	2	3	0	5	1	4	0	25874.090(50)	−24
2	1	1	0	2	0	2	0	11629.509(10)	−2	3	2	2	0	3	1	2	1	26299.640(50)	59
5	1	5	1	4	2	2	1	11806.400(500)	−313	4	2	2	1	4	1	3	1	26820.740(50)	−74
4	2	2	0	4	1	3	0	26821.570(50)	27	3	2	2	1	3	1	3	1	33314.260(50)	−49
5	1	4	1	4	2	3	1	26837.720(50)	−31	3	2	1	1	3	1	3	0	34992.500(50)	133
3	1	3	0	2	1	2	1	27590.180(50)	155	5	0	5	1	4	1	3	0	35136.480(50)	−44
2	2	1	0	2	1	1	1	27667.600(50)	95	4	2	3	0	4	1	4	0	35269.170(50)	188
3	2	1	1	3	1	2	1	27979.950(50)	90	4	2	3	1	4	1	4	1	35278.720(50)	−12
3	2	1	0	3	1	2	0	27984.520(50)	6	4	1	4	0	3	1	3	1	37175.250(50)	23
4	0	4	1	3	1	2	0	27986.060(50)	57	4	2	2	1	4	1	4	0	37581.210(50)	−59
3	0	3	0	2	0	2	1	28777.720(50)	−16	5	2	4	0	5	1	5	0	37736.430(50)	88
2	1	2	1	1	0	1	1	28995.980(50)	18	5	2	4	1	5	1	5	1	37738.720(50)	86
2	1	2	0	1	0	1	0	29003.430(50)	95	3	1	3	1	2	0	2	1	37739.700(50)	90
3	2	2	1	3	1	2	0	29015.190(50)	50	3	1	3	0	2	0	2	0	37749.850(50)	−91
3	2	2	0	2	2	1	1	29043.810(50)	73	4	0	4	0	3	0	3	1	38538.270(50)	−75
2	2	0	1	2	1	1	1	29091.760(50)	21	5	2	3	0	5	1	5	1	38593.940(50)	61
2	2	0	0	2	1	1	0	29095.370(50)	20	4	2	2	0	3	2	1	1	39760.370(50)	129
3	2	1	0	2	2	0	1	29302.530(50)	−64	4	1	4	1	3	1	3	0	39872.190(50)	48
3	1	3	1	2	1	2	0	30301.500(50)	56	4	2	3	1	3	2	2	0	41838.820(50)	33
2	2	1	1	2	1	1	0	30389.110(50)	330	3	1	2	0	2	0	2	1	42038.880(50)	101
3	1	2	0	2	1	1	1	30409.910(50)	91	5	0	5	1	4	1	4	1	43195.440(50)	−7
2	1	1	0	1	0	1	1	30465.630(50)	74	5	0	5	0	4	1	4	0	43200.400(50)	118
3	0	3	1	2	0	2	0	31499.010(50)	35	4	1	3	1	3	1	2	0	43636.550(50)	36
3	2	2	1	2	2	1	0	31757.300(50)	−155	3	1	2	1	2	0	2	0	44762.530(50)	82
2	2	1	0	2	1	2	0	31858.310(50)	12	4	1	4	1	3	0	3	1	46123.140(50)	32
3	2	1	1	2	2	0	0	32017.300(50)	−147	4	1	4	0	3	0	3	0	46137.150(50)	49
3	2	1	0	3	1	3	1	32283.670(50)	−13	5	1	5	0	4	1	4	1	46711.550(50)	137
4	0	4	1	3	1	3	1	32285.170(50)	−1	2	2	0	0	1	1	0	1	48941.790(50)	32
4	0	4	0	3	1	3	0	32287.460(50)	81	5	0	5	0	4	0	4	1	48090.320(50)	−17
5	0	5	0	4	1	3	1	32439.690(50)	−137	5	2	4	0	4	2	3	1	49169.020(50)	−3
3	1	2	1	2	1	1	0	33132.990(50)	53	5	3	2	1	5	2	3	1	49182.760(50)	−193
2	1	1	1	1	0	1	0	33194.230(50)	102	5	3	2	0	5	2	3	0	49185.410(50)	9
2	2	0	1	2	1	2	0	33282.520(50)	−12	5	1	5	1	4	1	4	0	49387.980(50)	−2
3	2	2	0	3	1	3	0	33312.050(50)	−37	3	3	0	0	3	2	2	1	49426.700(50)	165

[a] Obs is the observed frequency in MHz. The uncertainty is given in parentheses in kHz.

[b] Diff is the observed minus calculated frequency in kHz corresponding to the constants in Table 5.

TABLE 4—*Continued*

J'	K_a'	K_c'	v'	J''	K_a''	K_c''	v''	Obs[a]	Diff[b]	J'	K_a'	K_c'	v'	J''	K_a''	K_c''	v''	Obs[a]	Diff[b]
5	4	1	0	4	4	0	1	49482.250(50)	−95	4	1	3	1	3	0	3	0	56897.680(50)	123
5	3	3	0	4	3	2	1	49522.220(50)	−38	3	2	1	0	2	1	1	1	58394.370(50)	37
5	3	2	0	4	3	1	1	49581.070(50)	39	6	1	6	1	5	1	5	0	58844.470(50)	33
4	3	1	0	4	2	3	1	49619.300(50)	95	6	2	5	0	5	2	4	1	59171.600(50)	−59
2	2	1	0	1	1	1	1	49818.780(50)	82	3	2	2	1	2	1	1	1	59425.100(50)	141
4	3	1	1	4	2	2	1	50004.920(50)	−41	3	2	2	0	2	1	1	0	59432.580(50)	63
4	3	1	0	4	2	2	0	50017.410(50)	−62	6	4	2	0	5	4	1	1	59699.610(50)	−122
2	2	1	1	1	1	0	1	50235.280(50)	92	6	3	4	0	5	3	3	1	59749.330(50)	−45
2	2	1	0	1	1	0	0	50243.190(50)	109	6	3	3	0	5	3	2	1	59904.230(50)	278
5	2	3	0	4	2	2	1	50400.490(50)	−102	3	2	2	0	2	1	2	1	60902.210(50)	98
5	3	3	1	5	2	3	0	50444.680(50)	−44	3	2	1	1	2	1	1	0	61112.780(50)	−17
3	3	0	1	3	2	1	1	50450.340(50)	67	6	2	4	0	5	2	3	1	61167.640(50)	−68
3	3	0	0	3	2	1	0	50457.260(50)	99	6	1	5	0	5	1	4	1	61665.350(50)	−136
3	3	1	1	3	2	2	1	50772.810(50)	84	6	2	5	1	5	2	4	0	61834.560(50)	50
5	0	5	1	4	0	4	0	50780.210(50)	1	6	4	3	1	5	4	2	0	62347.990(50)	281
2	2	0	1	1	1	1	1	51242.850(50)	−82	6	4	2	1	5	4	1	0	62351.410(50)	39
2	2	0	0	1	1	1	0	51249.300(50)	−46	6	1	6	1	5	0	5	1	62360.440(50)	36
5	3	3	0	5	2	4	0	51296.400(50)	−318	6	1	6	0	5	0	5	0	62383.980(50)	5
4	3	2	1	4	2	2	0	51341.630(50)	−120	6	3	4	1	5	3	3	0	62418.300(50)	−17
5	1	4	0	4	1	3	1	51347.180(50)	−111	6	3	3	1	5	3	2	0	62574.300(50)	13
2	2	0	1	1	1	0	0	51667.330(50)	14	3	2	1	1	2	1	2	1	62582.490(50)	98
3	3	1	1	3	2	1	0	51803.270(50)	−82	3	2	1	0	2	1	2	0	62585.230(50)	103
5	2	4	1	4	2	3	0	51857.570(50)	−64	3	2	2	1	2	1	2	0	63615.700(50)	−53
3	3	0	1	3	2	2	0	52130.610(50)	57	6	2	4	1	5	2	3	0	63847.680(50)	−64
5	3	3	1	4	3	2	0	52204.110(50)	−152	7	0	7	1	6	1	6	1	64364.000(50)	−13
4	3	1	1	4	2	3	0	52317.290(50)	42	6	1	5	1	5	1	4	0	64364.970(50)	−194
2	2	1	1	1	1	1	0	52542.860(50)	84	7	0	7	0	6	1	6	0	64386.130(50)	−7
6	1	6	0	5	1	5	1	56196.380(50)	105	7	1	7	0	6	1	6	1	65636.870(50)	−38

obtained in the analysis as well as their uncertainty. These parameters include the rotational and first-order distortion constants corresponding to a Watson-type rotational Hamiltonian written in the *S* reduction. The I^l representation was used in the present analysis as in the previous one (*5*). The other parameters are relevant to the large-amplitude motion. The parameter

TABLE 5
Molecular Parameters[a] for the *g′Gg* Conformer of Ethylene Glycol

Parameter		Value	Parameter		Value
A		15 214.601(5)	h_{2v}		683.700(4)
B		5 538.331 6(29)	h_{2k}	$\times 10^3$	899.33(170)
C		4 595.025(2)	h_{2j}	$\times 10^3$	16.916(830)
			f_2	$\times 10^3$	−1.257 3(5300)
D_K	$\times 10^3$	74.603 8(6700)			
D_{JK}	$\times 10^3$	−31.714 3(2400)	θ_2		2.472 93(246)
D_J	$\times 10^3$	−7.170 6(430)	ϕ_2		91.205 9(18)
d_1	$\times 10^3$	2.198(35)			
d_2	$\times 10^3$	−0.21(3)			

[a] All parameters are in MHz, except θ_2 and ϕ_2, which are in degrees. Numbers in parentheses are one standard deviation in the same units as the last digit.

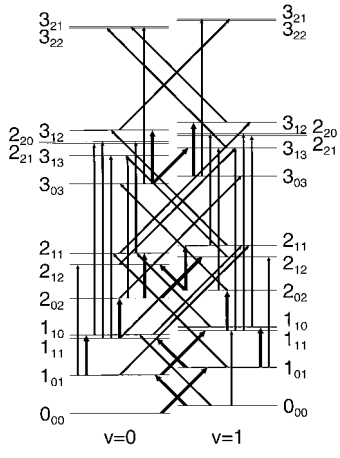

FIG. 3. Energy levels of the $J \leq 3$ levels in the *g′Gg* conformer of ethylene glycol with measured MWMWDR transitions. Rotational levels are indicated by thin horizontal lines and are labeled with J, K_a, and K_c. The left stack corresponds to $v = 0$ tunneling sublevels; the right stack corresponds to $v = 1$ tunneling sublevels. Thick (thin) arrows indicate the pump (signal) transitions considered in the double-resonance experiment.

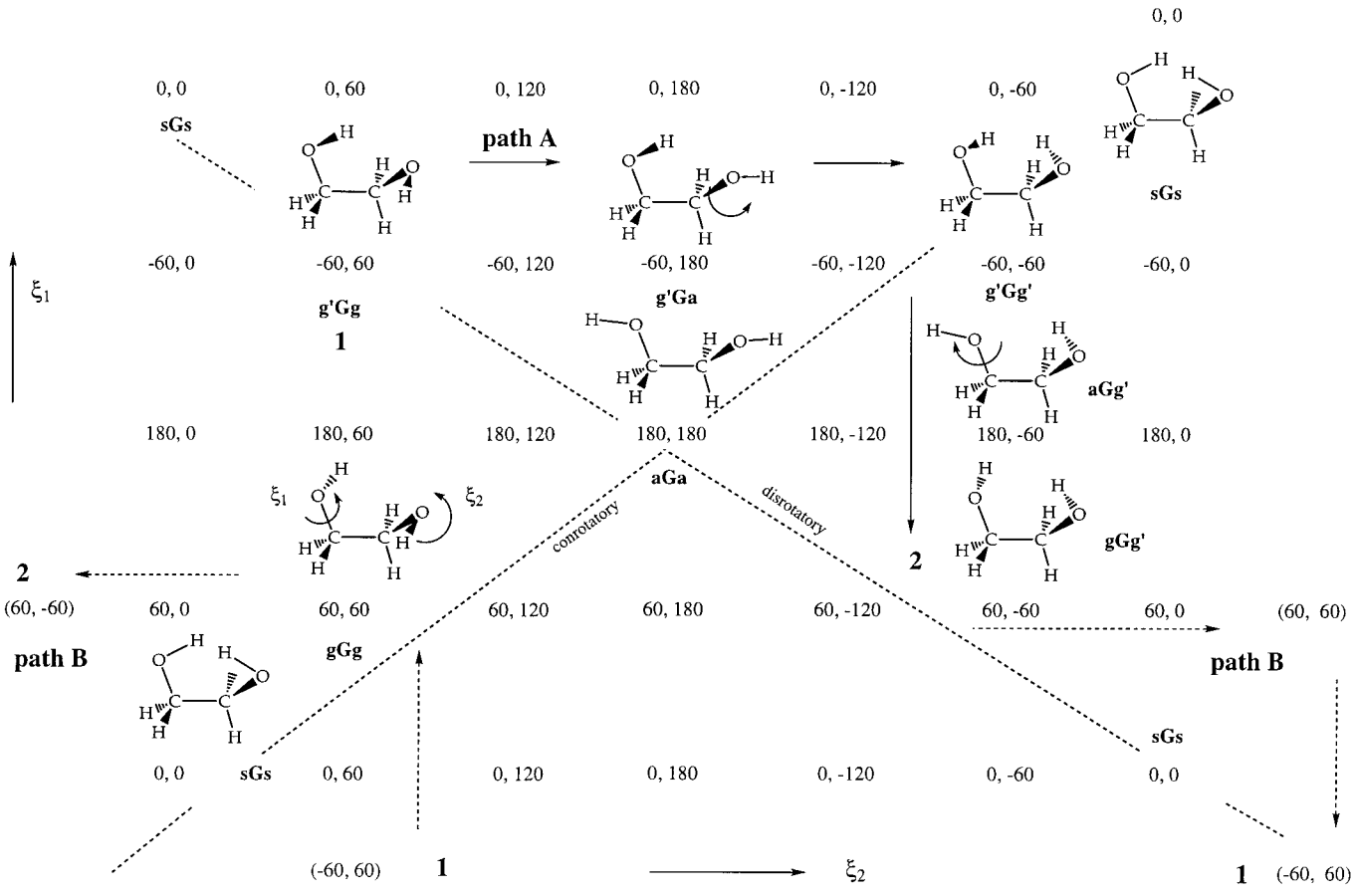

FIG. 4. Schematic drawing of the conformational energy surface (CES) spanned by the rotational angles ξ_1 and ξ_2. A grid of (ξ_1, ξ_2) points is given where for selected points the conformations investigated are shown. Two concerted paths (conrotatory and disrotatory) are indicated by dashed lines. The nonconcerted flip-flop rotation of the $g'Gg$ conformer, labeled **1**, to the gGg' conformer, labeled **2**, can proceed either via path *A* (long path) or via path *B* (short path).

h_{2v} is such that $2 \times h_{2v}$ is the tunneling splitting for $J = 0$. The parameters h_{2k} and h_{2j} account for distortion effects on the tunneling splitting. Finally, the angles θ_2 and ϕ_2 describe the rotational dependence of the tunneling splitting and are such that the Eulerian-type rotation,

$$S^{-1}(\phi_2 + \pi,\ \theta_2,\ \phi_2), \qquad [1]$$

is the rotation through which the whole molecule must be rotated in order to cancel the angular momentum generated along the tunneling path (*5*, *24*, *25*). The present analysis does not allow us to carry out a unique determination of the angle ϕ_2 since, as can be gathered from Eqs. [8] and [9] of Ref. (*5*), making the substitution $\phi_2 \rightarrow \pi - \phi_2$ does not alter the energy levels but merely changes a phase factor in the Hamiltonian matrix. The values of the angles θ_2 and ϕ_2 will nonetheless help us to discriminate between path *A* and path *B* and this will be discussed in the following section.

6. THE ROLE OF H BONDING AND TUNNELING FOR THE CONFORMATIONAL BEHAVIOR

The results of the *ab initio* calculations at the MP2/6-311G(*d*, *p*) level are summarized in Table 6 (relative energies and enthalpies) and in Table 7 and Fig. 6 (MP2 geometries) and used in the following to investigate the CES of glycol and to obtain information on the tunneling path the molecule takes when it interconverts from one conformer to the other using either path *A* or path *B* as schematically shown in Fig. 4.

In the *ab initio* calculations, seven stationary points were determined and the 24 internal coordinates of the molecule were calculated. Three of these stationary points are true minima (Table 6) corresponding to the $g'Ga(aGg')$, $g'Gg(gGg')$, and gGg conformers. The four other stationary points are first-order or second-order saddle points as documented by the number of imaginary frequencies. One of them is the $g'Gg'$ conformation located on path *A*; the two other ones will be labeled *TS1* and *TS2*, while the second-order transition state is denoted as *TS3*. Figure 5 illustrates qualitatively these results where an arbitrary CES contour plot is

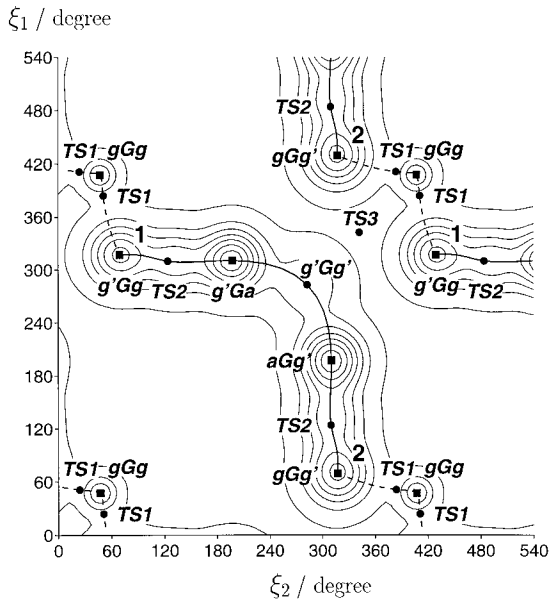

FIG. 5. An arbitrary conformational energy surface (CES), plotted against the two angular coordinates ξ_1 and ξ_2, illustrates the results of the *ab initio* calculations. The true minima of the CES are indicated by full squares while full circles correspond to saddle points. Relative energies of these points are listed with regard to the E + ZPE values in Table 6. The solid line connecting conformers **1** and **2** represents tunneling path *A*. The dotted line, also connecting conformers **1** and **2**, illustrates the hypothetical tunneling path *B*. Compare with Fig. 4.

shown along with the calculated stationary points and the tunneling paths described in the previous sections.

The calculated energies, enthalpies, and free enthalpies all identify the $g'Ga$ conformer to be more stable than the $g'Gg$ conformer ($\Delta E = 0.09$ kcal/mol, Table 6), in line with results published by Teppen and co-workers obtained with a similar approach (*17*). However, contrary to these authors, we determined also the zero-point energy difference between the $g'Gg$ and $g'Ga$ to be ΔZPE = 0.23 kcal/mol at the MP2/6-311G(*d*, *p*) level of theory. The sum energy difference plus zero-point energy difference is equal to 0.32 kcal/mol and is in excellent agreement with the experimental value of 0.33 ± 0.1 kcal/mol measured by Kristiansen *et al.* (*3*). These authors speak in their publication of an internal energy difference based on a comparison of MW intensities. We note that experiments were carried out under Boltzmannian equilibrium conditions and, therefore, any intensity measurement can only give information on the population of the two conformers and by this on the total energy difference which is the sum of the difference (ΔE) between the two points of the PES corresponding to the $g'Gg$

TABLE 6
MP2/6-311G(*d*, *p*) Energies and Enthalpies of Some Ethylene Glycol Forms with a *G* Conformation[a]

Form	ΔE	$\Delta H(298)$	ZPE	S	$\Delta G(298)$	NI
$g'Ga$	−229.781 92	−229.688 43	54.98	69.44	−229.721 43	0
$g'Gg$	0.09	0.17	55.21	68.61	0.42	0
gGg	3.18	3.04	54.70	69.28	3.09	0
TS1	3.33	2.56	54.40	68.61	2.81	1
TS2	1.47	0.81	54.61	67.84	1.28	1
TS3	6.12	4.60	53.94	65.41	5.81	2
$g'Gg'$	1.72	0.95	54.44	67.02	1.67	1

[a] Relative energies ΔE, relative enthalpies $\Delta H(298)$, Zero Point Energies (ZPE), relative free enthalpies $\Delta G(298)$ in kcal/mol, and entropies S in cal/(mol · Kelvin). For the reference form $g'Ga$ absolute energy and enthalpy are given in hartrees (= 627.52 kcal/mol). NI denotes the number of imaginary frequencies.

TABLE 7
MP2/6-311G(*d*, *p*) Geometries of Several Stationary Points[a] Investigated in this Work

Parameter[b]	gGg	*TS1*	*TS2*	*TS3*	$g'Gg'$
C_0–C_1	1.519	1.519	1.515	1.512	1.518
C_1–O_7	1.414	1.417	1.430	1.425	1.422
C_0–O_6	1.414	1.416	1.413	1.425	1.422
C_0–H_4	1.100	1.099	1.093	1.093	1.093
C_0–H_2	1.095	1.096	1.099	1.098	1.097
C_1–H_5	1.100	1.099	1.096	1.093	1.093
C_1–H_3	1.095	1.094	1.094	1.098	1.097
O_7–H_9	0.960	0.960	0.956	0.958	0.959
O_6–H_8	0.960	0.959	0.962	0.958	0.959
$\angle O_7C_1C_0$	113.2	112.6	107.7	112.6	110.8
$\angle O_6C_0C_1$	113.2	112.8	110.4	112.6	110.8
$\angle H_4C_0C_1$	108.6	108.6	110.4	109.6	110.2
$\angle H_2C_0C_1$	109.7	109.6	108.9	108.8	109.4
$\angle H_5C_1C_0$	108.6	109.2	110.4	109.6	110.2
$\angle H_3C_1C_0$	109.7	109.7	109.4	108.8	109.4
$\angle H_2C_0O_6$	105.6	106.7	111.3	109.8	110.9
$\angle H_3C_1O_7$	105.6	105.3	108.5	109.8	110.9
$\angle H_4C_0O_6$	112.1	111.3	107.2	107.5	107.0
$\angle H_5C_1O_7$	112.1	112.2	111.8	107.5	107.0
$\angle H_9O_7C_1$	106.6	106.6	107.8	107.7	105.5
$\angle H_8O_6C_0$	106.6	106.6	104.4	107.7	105.5
$\angle O_6C_0C_1O_7$	51.3	48.5	56.3	67.8	56.9
$\angle H_9O_7C_1C_0$	47.3	51.0	124.0	−17.8	−77.4
$\angle H_8O_6C_0C_1$	47.3	23.8	−50.4	−17.8	−77.4

[a] The gGg form corresponds to a true minimum. The *TS1*, *TS2*, *TS3*, and $g'Gg'$ forms are first order or second order saddle points, as indicated in Table 6.

[b] In this column structural parameters are given. Bond distances and bond angles are respectively given in Å and degree units. The atom numbering is defined in Fig. 2.

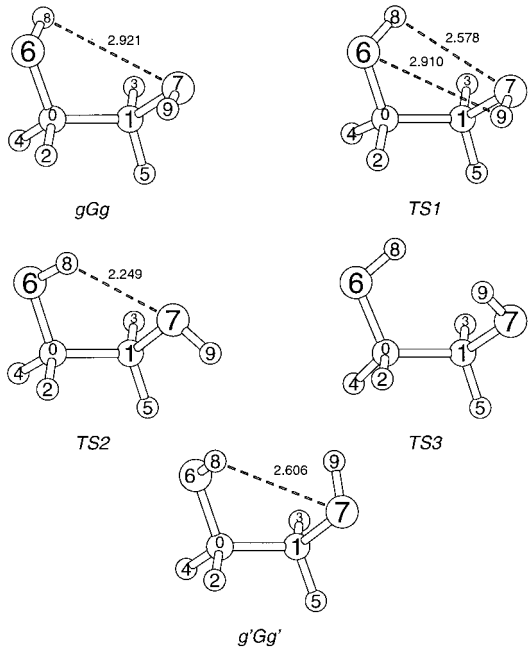

FIG. 6. *Ab initio* MP2/6-311G(*d*, *p*) geometries for the conformations of ethylene glycol investigated in this work. Distances are in Å. Nonbonded interactions between the OH groups are indicated by dashed lines. Conformations *gGg*, *TS3*, and $g'Gg'$ have a twofold axis of symmetry.

and $g'Ga$ plus the difference in zero-point energy (ΔZPE) between the two conformers.

Even though there is good agreement between observed and calculated total energy difference, in view of the smallness of the energy difference ΔE compared to the zero-point energy difference ΔZPE, we cannot exclude that $g'Gg$ and $g'Ga$ actually possess the same energy. In this connection it is interesting to note that all previous quantum chemical work on ethylene glycol (*6, 8–22*) failed to calculate stability differences of its conformers at a consistent, sufficiently high level of *ab initio* theory such as that carried out in this work (geometries, energies, vibrational frequencies, enthalpies, entropies, free enthalpies all at the MP2/6-311G(*d*, *p*) level), not to speak of the fact that rotational TSs of the molecule were never calculated before. So far, the present investigation can be considered to represent the most reliable *ab initio* investigation on ethylene glycol ever published.

The two conformers are separated by a rotational barrier of 1.47 kcal/mol (1.38 kcal/mol for the reverse rotation; activation enthalpies: 0.81 and 0.64 kcal/mol, Table 6) defined by the energy of *TS2*, which is located at $(\xi_1, \xi_2) = (-50.4, 124)$, thus indicating that during the rotation of the O_7H_9 group the position of O_6H_8 group is only slightly adjusted. Conversion of the $g'Ga$ conformer into the equivalent aGg' conformer requires an increase in the energy by 1.72 kcal/mol to surmount the barrier located at $(-77.4, -77.4)$; activation enthalpy: 0.95 kcal/mol, Table 6, and populated by a $g'Gg'$ form. Hence, the interconversion **1** → **2** along path *A* passes three saddle points *TS2*, $g'Gg'$, and *TS2*, where the $g'Gg'$ barrier is slightly higher than the *TS2* barriers as can be gathered from Table 6.

Rotation along path *B* leads from **1** to *TS1* (3.33 kcal/mol), then to a local minimum occupied by a *gGg* form (3.18 kcal/mol) and via another *TS1* to **2** (see Fig. 5). The data listed in Table 6 reveal that after ZPE corrections the *gGg* minimum transforms into a transition state, which is at 2.91 kcal/mol ($\Delta H(298) = 3.04$; $\Delta G(298) = 3.09$ kcal/mol) and by this more than twice as large as the barrier at *TS2*. Hence, *ab initio* theory clearly predicts path *B* to be energetically unfavorable.

The OH group donating an H atom in the H bond, which will be henceforth denoted *D* group, has to be distinguished from the H-accepting OH group, denoted henceforth *AC* group. Considering the difference in free enthalpy values of the TSs for path *A* and path *B*, more than 90% of the ethylene glycol molecules tunnel from the $g'Gg$ conformer to reach the gGg' conformer, which implies an initial rotation of the *AC* group O_7H_9 (Fig. 4). This is a direct consequence of the fact that the *D* group O_6H_8 prefers to keep its position as long as possible.

Investigation of the electron density distribution and the associated Laplace concentration of the lone pairs at the *AC* group O atom shows that in the $g'Ga$ and $g'Gg$ conformers the *D* group orients its H atom exactly in the direction of one of the electron lone pairs at the *AC* group. The distance between the H of the *D* group and the O of the *AC* group is just 2.26 Å (Fig. 2), which as a consequence of two vicinal OH groups is some 0.2 Å smaller than observed for intermolecular H-bonding (*40*).

Calculation of the adiabatic OH stretching and CC—OH torsional force constants and frequencies (these are related to the OH bond strength and the magnitude of the barrier for rotation at CC—OH) reveals that there are characteristic differences between *D* and *AC* groups as emphasized by Table 8. The OH bond of the *D* group is weakened and that of the *AC* group strengthened relative to suitable reference OH groups without any possibility of H bonding as for example in the *gGg* form. Similarly, rotation is much easier for the *AC* group than for the *D* group as is indicated by the adiabatic torsional frequencies of 488 and 259 cm^{-1} of *D* and *AC* groups, respectively, in the $g'Ga$ conformer. The differences between *D* group and *AC* group decrease when the molecule is rotated from the $g'Ga$ into the $g'Gg$ form (Table 8), indicating that although H bonding still exists in the latter form it is weakened because of geometrical limitations.

If one considers that the lone-pair region at an O atom may stretch over 120–150° on the backside of the C—O—H unit, then it will be easy to understand that relatively small adjustments in the *D* group position can keep H bonding intact during a 120–150° rotation of the *AC* group, while on the other hand just a 10° rotation of the *D* group weakens the H bond significantly due to a relatively strong increase of the H(*D* group)—O(*AC* group) distance. This is the reason

TABLE 8
Calculated Adiabatic Internal Mode Frequencies and Force Constants of Donor and Acceptor OH Groups for Some Selected Ethylene Glycol Conformers[a]

	$g'Ga$		$g'Gg$		gGg	
Parameter	ω^b	k^c	ω^b	k^c	ω^b	k^c
D OH stretch	3862	8.33	3850	8.28	3897	8.48
AC OH stretch	3923	8.60	3882	8.42		
D torsion	488	0.10	484	0.10	295	0.03
AC torsion	259	0.03	409	0.07		
Δ stretch	61	0.27	32	0.14		
Δ torsion	−229	−0.07	−75	−0.03		

[a] Frequencies and force constants calculated at MP2/6-311G(d, p). D and AC denote donor and acceptor OH groups; D OH stretch (AC OH stretch) refers to the stretching motion of the donor (acceptor); D torsion (AC torsion) to the torsional motion of the donor (acceptor); Δ stretch and Δ torsion to the difference between acceptor and donor with regard to the quantity indicated.
[b] Frequencies are given in cm^{-1}.
[c] Force constants are given in N/cm for stretching modes and in 10^{-16} N · cm/rad^2 for torsional modes.

the molecule prefers the longer path A as shown in Fig. 5 where tunneling is first almost parallel to the ξ_2 axis. There is also no possibility for the molecule of following the conrotatory path from $g'Gg'$ via *TS3* and by this changing from path A to path B. *TS3* is a second-order transition state of relatively high energy (6 kcal/mol, Table 6), which the molecule will not pass.

The unfeasibility of path B (dashed line in Fig. 5) is confirmed when the angles θ_2 and ϕ_2, reported in Table 5, are calculated theoretically starting from the above tunneling paths and compared to the values obtained in the analysis. A similar calculation was carried out in Section 5 of Ref. (*5*) and requires a path parameterization of chosen internal coordinates of the molecule along the path in terms of the path coordinate η equal to -1 at conformer **1** and to $+1$ at conformer **2** (see Ref. (*24*)). In this investigation all 24 internal coordinates of the molecule were expressed in terms of η. This is illustrated in Fig. 7 where the torsional angles ξ_1 and ξ_2 are plotted as a function of η for both path A and path B. Theoretically calculated values for the angles θ_2 and ϕ_2 are given in Table 9, where the values obtained in the analysis are also listed. Even though the value of ϕ_2 could not be unambiguously determined (see Section 5), there is satisfactory agreement for path A but not for path B. This further confirms that the feasible path displayed by the $g'Gg$ is indeed path A.

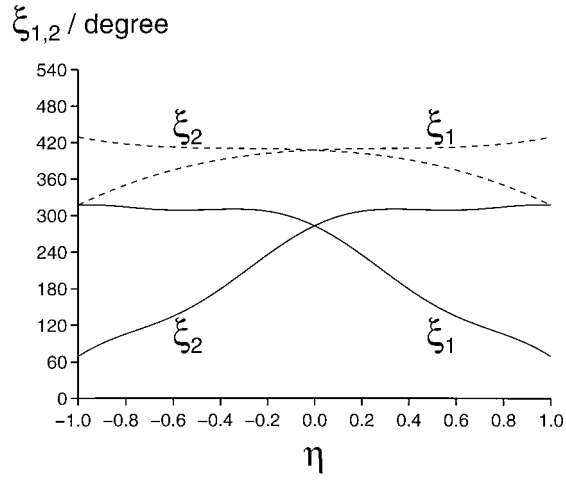

FIG. 7. The angles ξ_1 and ξ_2 are plotted as a function of the unitless path coordinate η for path A and B. Conformers **1** and **2** are given by $\eta = -1$ and $\eta = +1$, respectively. Solid lines correspond to path A; dashed lines correspond to path B. The fact that for path A both OH groups are rotated by a larger amount than for path B is obvious.

7. CONCLUSIONS

With the use of MBFTMW and MWMWDR techniques it was possible to assign and to analyze rotation–torsion frequencies of the $g'Gg$ conformer of ethylene glycol. Furthermore, it was possible to combine the experimental data with *ab initio* calculations to yield unequivocal evidence for the tunneling path of the $g'Gg$ as well as for the $g'Ga$ conformers leading to their symmetrically equivalent counterparts (gGg' and aGg', respectively). Thus, for the first time, a more global

TABLE 9
Numerical Values for the Angles θ_2 and ϕ_2

Path[a]	θ_2	ϕ_2
A	2.946°	91.753°
B	1.525°	88.010°
Analysis	2.473°	91.206°

[a] In this column, the letters A and B are used to identify the path. 'Analysis' indicates that the values given are those, reported in Table 5, obtained from the analysis of the microwave data.

view of the potential energy surface of ethylene glycol has evolved.

ACKNOWLEDGMENTS

Professor Collin Marsden, University of Montpellier, carried out *ab initio* calculations to start the project. His help is warmly acknowledged. Research was supported by the Swedish Natural Science Research Council (NFR). All calculations were done on the CRAY C90 of the Nationellt Superdatorcentrum (NSC), Linköping, Sweden. D.C. thanks the NSC for a generous allotment of computer time. We are also grateful to Angelica Hight Walker and Rick D. Suenram, Molecular Spectroscopy Division, NIST, for the recording of MBFTMW transitions that put this project on the right tracks.

REFERENCES

1. E. Walder, A. Bauder, and Hs. H. Günthard, *Chem. Phys.* **51,** 223–239 (1980).
2. W. Caminati and G. Corbelli, *J. Mol. Spectrosc.* **90,** 572–578 (1981).
3. P.-E. Kristiansen, K.-M. Marstokk, and H. Møllendal, *Acta Chem. Scand. Ser. A* **41,** 403–414 (1987).
4. K.-M. Marstokk and H. Møllendal, *J. Mol. Struct. (Theochem)* **22,** 301–303 (1974).
5. D. Christen, L. H. Coudert, R. D. Suenram, and F. Lovas, *J. Mol. Spectrosc.* **172,** 57–77 (1995).
6. M. R. Kazerouni, L. Hedberg, and K. Hedberg, *J. Am. Chem. Soc.* **119,** 8324–8331 (1997).
7. H. Takeuchi and M. Tasumi, *Chem. Phys.* **77,** 21–34 (1983).
8. T.-K. Ha, H. Frei, R. Meyer, and Hs. H. Günthard, *Theor. Chim. Acta* **34,** 277–292 (1974).
9. C. van Alsenoy, L. van den Enden, and L. Schäfer, *J. Mol. Struct. (Theochem)* **108,** 121–128 (1984).
10. B. J. C. Cabral, L. M. P. C. Albuquerque, and F. M. S. S. Fernandes, *Theor. Chem. Acta* **78,** 271–280 (1991).
11. P. I. Nagy, W. J. Dunn, III, G. Alagona, and C. Ghio, *J. Am. Chem. Soc.* **113,** 6719–6729 (1991).
12. P. I. Nagy, W. J. Dunn, III, G. Alagona, and C. Ghio, *J. Am. Chem. Soc.* **114,** 4752–4758 (1992).
13. S. A. Vazquez, M. A. Rios, and L. Carballeira, *J. Comput. Chem.* **13,** 851–859 (1992).
14. M. A. Murcko and R. A. DiPaoloa, *J. Am. Chem. Soc.* **114,** 10010–10018 (1992).
15. T.-S. Yeh, Y.-P. Chang, T.-M. Su, and I. Chao, *J. Phys. Chem.* **98,** 8921–8929 (1994).
16. T. Oie, I. A. Topol, and S. K. Burt, *J. Phys. Chem.* **98,** 1121–1128 (1994).
17. B. J. Teppen, M. Cao, R. F. Frey, C. van Alsenoy, D. M. Miller, and L. Schäfer, *J. Mol. Struct. (Theochem)* **314,** 169–190 (1994).
18. C. C. Cramer and D. G. Truhlar, *J. Am. Chem. Soc.* **116,** 3892–3900 (1994).
19. P. Bultinck, A. Goeminne, and D. Van de Vondel, *J. Mol. Struct. (Theochem)* **357,** 19–32 (1995).
20. G. I. Csonka and I. G. Csizmadia, *Chem. Phys. Lett.* **243,** 419–428 (1995).
21. S. Reiling, J. Brickmann, M. Schlenkrich, and P. A. Bopp, *J. Comput. Chem.* **17,** 133–147 (1996).
22. G. Alagona and C. Ghio, *J. Mol. Struct. (Theochem)* **254,** 287–300 (1992).
23. S. Wolfe, *Acc. Chem. Res.* **5,** 102–111 (1972).
24. J. T. Hougen, *J. Mol. Spectrosc.* **114,** 395–426 (1985).
25. L. H. Coudert and J. T. Hougen, *J. Mol. Spectrosc.* **130,** 86–119 (1988).
26. R. G. Parr and W. Yang, *in* "International Series of Monographs on Chemistry 16: Density-Functional Theory of Atoms and Molecules," Oxford University Press, New York, 1989.
27. P. Gill, *in* "Encyclopedia of Computational Chemistry" (P. V. R. Schleyer, N. L. Allinger, T. Clark, J. Gasteiger, P. A. Kollman, H. F. Schaefer, III, and P. R. Schreiner, Eds.), Vol. 1, p. 678, Wiley, Chichester, 1998.
28. D. Cremer, *in* "Encyclopedia of Computational Chemistry" (P. V. R. Schleyer, N. L. Allinger, T. Clark, J. Gasteiger, P. A. Kollman, H. F. Schaefer, III, and P. R. Schreiner, Eds.), Vol. 3, p. 1706, Wiley, Chichester, 1998.
29. A. D. Becke, *J. Chem. Phys.* **98,** 5648–5652 (1993).
30. P. C. Hariharan and J. A. Pople, *Chem. Phys. Lett.* **16,** 217–219 (1972).
31. J. J. Nova and C. Sosa, *J. Phys. Chem.* **99,** 15837–15845 (1995).
32. R. Wrobel, W. Sander, E. Kraka, and D. Cremer, *J. Phys. Chem. A* **103,** 3693–3705 (1999).
33. Z. Konkoli and D. Cremer, *Int. J. Quantum Chem.* **67,** 1–9 (1998).
34. D. Cremer, J. A. Larsson, and E. Kraka, *in* "Theoretical and Computational Chemistry" (C. Párkányi, Ed.), Vol. 5, p. 259, Elsevier, Amsterdam/New York, 1998.
35. Z. Konkoli, J. A. Larsson, and D. Cremer, *Int. J. Quantum Chem.* **67,** 11–27 (1998).
36. J. A. Larsson and D. Cremer, *J. Mol. Struct. (Theochem)* **385,** 485–486 (1999).
37. E. Kraka, J. Gräfenstein, J. Gauss, F. Reichel, L. Olsson, Z. Konkoli, Z. He, Y. He, and D. Cremer, COLOGNE99, Göteborg University, Göteborg, 1999.
38. M. J. Frisch, G. W. Trucks, H. B. Schlegel, G. E. Scuseria, M. A. Robb, J. R. Cheeseman, V. G. Zakrzewski, J. A. Montgomery, Jr., R. E. Stratmann, J. C. Burant, S. Dapprich, J. M. Millam, A. D. Daniels, K. N. Kudin, M. C. Strain, O. Farkas, J. Tomasi, V. Barone, M. Cossi, R. Cammi, B. Mennucci, C. Pomelli, C. Adamo, S. Clifford, J. Ochterski, G. A. Petersson, P. Y. Ayala, Q. Cui, K. Morokuma, D. K. Malick, A. D. Rabuck, K. Raghavachari, J. B. Foresman, J. Cioslowski, J. V. Ortiz, B. B. Stefanov, G. Liu, A. Liashenko, P. Piskorz, I. Komaromi, R. Gomperts, R. L. Martin, D. J. Fox, T. Keith, M. A. Al-Laham, C. Y. Peng, A. Nanayakkara, C. Gonzalez, M. Challacombe, P. M. W. Gill, B. Johnson, W. Chen, M. W. Wong, J. L. Andres, C. Gonzalez, M. Head-Gordon, E. S. Replogle, and J. A. Pople, "GAUSSIAN98, Revision A.3," Gaussian, Inc., Pittsburgh, PA, 1998.
39. R. S. Ruoff, T. D. Klots, T. Emilsson, and H. S. Gutowsky, *J. Chem. Phys.* **93,** 3142–3150 (1990).
40. J. E. Del Bene, *in* "Encyclopedia of Computational Chemistry" (P. V. R. Schleyer, N. L. Allinger, T. Clark, J. Gasteiger, P. A. Kollman, H. F. Schaefer, III, and P. R. Schreiner, Eds.), Vol. 2, p. 1263. Wiley, Chichester, 1998.